ADVANCED MATERIALS INTERFACES
Open Access
www.advmatinterfaces.de

Check for updates

Hue-Resolved Strain Sensing in Mechanochromic Colloidal Photonic Crystal Films

*Yujin Lee, Seonu Lee, Chi Yeung Oh, Young-Seok Kim, Tae Soup Shim, and Hyerim Hwang**

Mechanochromic materials, particularly colloidal photonic crystals (CPCs) embedded in soft stretchable films, hold significant potential in applications requiring precise and real-time strain monitoring. These materials exhibit strain-induced color changes arising from alterations in lattice periodicity, yet conventional quantification methods like spectroscopy are often costly, complex, and challenging to scale. Here, an image-based quantification framework is presented that evaluates mechanochromic behavior with high precision by tracking hue shifts in optical images. CPC films are prepared from core-shell nanoparticles with acrylate shells of different glass transition temperatures, allowing systematic control of elastic modulus and composition-dependent chromatic responses. RGB image data are converted into the hue-saturation-value (HSV) color space, where the hue component serves as a robust optical readout of lattice compression, directly reflecting nanoscale spacing changes. The hue-strain relationship is reproducible, material-dependent, and consistent under multi-axial loading, thereby linking strain-induced color shifts to intrinsic material properties. Statistical filtering together with consistency across different brightness levels further ensures stability under variable imaging conditions. This framework establishes hue as a precise and scalable metric for mechanochromic quantification, broadening opportunities for cost-effective strain sensing in wearable devices, soft robotics, and structural diagnostics.

1. Introduction

Mechanochromic materials, known for their visible responses to mechanical stimuli, play an indispensable role in structural monitoring applications. Among these, colloidal photonic crystals (CPCs) embedded in stretchable films stand out as particularly promising.[1–4] These crystals exhibit structural colors through the coherent Bragg diffraction of light interacting with their periodically arranged lattice.[5–7] When the film is stretched or compressed, the periodic structure changes, resulting in visually detectable color shifts. This feature allows for precise and visually detectable strain monitoring, making these materials highly suitable for applications requiring both sensitivity and accuracy. For example, in wearable technology, these CPCs can continuously monitor strain and pressure, providing critical insights for medical diagnostics and personal health tracking.[8] In industrial settings, they serve as advanced strain sensors, enhancing the safety and reliability of mechanical systems by detecting deformations in real-time. The integration of CPCs into stretchable films greatly enhances the capabilities of mechanochromic materials, driving innovation across fields such as healthcare, manufacturing, and infrastructure monitoring.[9,10] Other mechanochromic systems include electrically responsive organogels and chiral liquid crystal elastomers, where color changes arise from molecular alignment or external actuation.[11–13]

Despite the significant potential of these materials, simply observing color changes with the naked eye only confirms that deformation has occurred, without offering any quantitative measure of strain. Spectroscopy can accurately measure the color shifts that correspond to changes in mechanical strain, but require costly, complex equipment, making them impractical for widespread use in applications that demand high accuracy and simplicity. The main challenge lies in measuring the dominant wavelength change precisely to determine the exact strain. Commission Internationale de l'Éclairage (CIE)-based approaches allow the estimation of dominant wavelengths or chromaticity coordinates from reflectance spectra, which requires additional processing.[13,14] Accurate colorimetric analysis from digital images remains challenging, as RGB values do not directly

Y. Lee, S. Lee, H. Hwang
Department of Chemical Engineering and Materials Science
Ewha Womans University
Seoul 03760, Republic of Korea
E-mail: hyerimhwang@ewha.ac.kr
C. Y. Oh, T. S. Shim
Department of Energy Systems Research
Ajou University
Suwon 16499, Republic of Korea
T. S. Shim
Department of Chemical Engineering
Ajou University
Suwon 16499, Republic of Korea
Y.-S. Kim
Display Research Center
Korea Electronics Technology Institute
Seongnam, Gyunggi-do 13509, Republic of Korea

The ORCID identification number(s) for the author(s) of this article can be found under https://doi.org/10.1002/admi.202500633

© 2025 The Author(s). Advanced Materials Interfaces published by Wiley-VCH GmbH. This is an open access article under the terms of the Creative Commons Attribution License, which permits use, distribution and reproduction in any medium, provided the original work is properly cited.

DOI: 10.1002/admi.202500633

translate to spectral data without device-specific modeling or spectral estimation. Calibration with color charts is often set-up dependent and limited by the use of non-reflective references, while regression and machine learning approaches require computational resources and large data sets, limiting their practical use.

To address these limitations, recent work has explored alternative color spaces that offer more robust and interpretable descriptors. Image analysis in spaces such as hue-saturation-value (HSV) or CIE Lab* has been successfully applied in fields including urinalysis, saliva-based alcohol testing, and water quality monitoring.[15–17] Image-based analysis has also been increasingly explored in photonic crystal sensing, where approaches based on RGB, chromaticity coordinates (CIE), or brightness tracking have been reported.[18–23] In this context, digital image analysis offers a simpler, cost-effective alternative by capturing real-time color changes using standard cameras. While RGB values are readily available, their complex structure hinders direct correlation with strain. Instead, hue which is one component of the HSV color space, directly corresponds to the dominant reflected wavelength perceived by the human eye. Although hue is not spectrally unique in the strict sense, since it is a perceptual category derived from RGB channels that only sample broad spectral regions, it provides a stable and reproducible proxy for strain-induced optical shifts when used in a relative manner. It is also worth noting that while absolute RGB values can vary depending on the camera's spectral response, the HSV conversion normalizes such differences, and relative hue changes remain consistent. Because structure color in CPCs arises from Bragg diffraction, strain-induced changes in lattice periodicity cause predictable wavelength shifts, which manifests as hue shifts. This allows hue to serve as a physically meaningful and intuitive optical readout of mechanical deformation. By converting RGB data into HSV space and isolating the hue component, we enable direct monitoring of photonic crystal compression under strain while minimizing the influence of lighting variation and device artifacts.

In this study, we develop a method to quantify the mechanochromic properties of CPC-based films with tunable elastic modulus values, aiming to establish a reliable platform for structural color evaluation. The films are fabricated by assembling core-shell nanoparticles with acrylate shells of different glass transition temperatures, enabling systematic control of mechanical properties and reproducible, material-specific chromatic responses under strain.[24] RGB data from the optical images were converted them into the HSV color space, with the hue component isolated to directly track the strain-induced color shifts. We validated this image-based approach against established evaluation standards in photonic crystal sensing, showing quantitative agreement in strain-wavelength sensitivity and reproducibility across different polymer compositions. We further show that the hue-strain correlation in these films remains consistent under multi-axial loading, directly linking lattice compression to optical response irrespective of in-plane direction. By connecting image-derived hue shifts to intrinsic material properties, our framework couples photonic crystal mechanics with hue-resolved quantification, thereby enabling reliable structure color evaluation and broadens the applicability of mechanochromic materials across diverse sensing platforms.

2. Results and Discussion

Soft CPC films exhibiting mechanochromic properties were fabricated using a melt-shear assembly process of polymer-coated colloidal nanoparticles (**Figure 1**a).[24] This method utilizes core-shell nanoparticles composed of a polystyrene (PS) core ($d \approx 200$ nm), a poly(methyl methacrylate) (PMMA) interlayer, and one of three different soft acrylate polymer shells: poly(ethyl acrylate) (PEA), poly(hexyl methacrylate) (PHMA), and poly(methyl acrylate) (PMA). These different acrylate shells provide varying mechanical properties, such as elastic modulus and glass transition temperature, which contribute to the films' distinctive mechanochromic responses. Through melt-shear assembly, the nanoparticles form ordered photonic crystal structures, which produce structural color via Bragg reflection. As illustrated in Figure 1b, when the tensile stress is applied to the film along its length, compressive forces are simultaneously exerted in the thickness direction, resulting in the shrinking of the crystal lattice. This change in lattice periodicity alters the film's optical properties, leading to a shift in the reflected wavelength, which manifests as visible color changes. Figure 1c further highlights this effect by showing a photograph of the CPC film under 30% strain (ε) alongside COMSOL simulations, which visualize local strain distributions under global deformations of $\varepsilon = 15\%$ and 30%. While local stress heterogeneities arise especially near the clamping zones, the mechanochromic response remains spatially coherent over the central region, which is the focust of hue analysis in this study.

The morphology and uniformity of the core-shell colloidal particles were confirmed by scanning electron microscopy (SEM), as shown in Figure S1 and Table S1 (Supporting Information). SEM analysis revealed monodisperse, spherical particles with total diameter of 245 nm (PEA shell), 231 nm (PHMA shell), and 244 nm (PMA shell), depending on the shell composition; the acrylate shell compositions were synthesized using a starved-feed emulsion polymerization (S1 in the Supporting Information, as reported in our prior work.[25] The effective refractive index (n_{eff}) of the CPC films, estimated by effective medium approximation (S2 in the Supporting Information). Bragg-Snell equation in colloidal crystals is described by $\lambda = 2d_{\text{hkl}}\sqrt{n_{eff}{}^2 - sin^2\theta}$, where d_{hkl} is the interplanar spacing and θ the external angle of incidence. For face-centered cubic (FCC) crystals, the (111) spacing is $d_{111} = \sqrt{2/3}\,D$ (with D the particle diameter), yielding: $\lambda = \sqrt{8/3}\;D\sqrt{n_{\text{eff}}{}^2 - sin^2\theta}$. A detailed derivation of this relation, starting from Bragg's law and adapted for three-dimensional photonic crystals, is provided in the S3 of the Supporting Information. Because of this dependence on θ, structural color in CPC films is inherently angle-dependent. In our experiments, optical measurements were performed under fixed, near-normal incidence to minimize angular variation in color (Figure S2, Supporting Information). While this angular sensitivity is a general characteristic of photonic crystals, its impact on real-world applications is often mitigated in compact or head-on configurations, such as localized strain sensors.

To generate visible structural color, the colloidal particles must exhibit an ordered arrangement with interparticle spacings on the order of visible wavelengths. SEM image in the Figure 1a confirm hexagonally packed domains with ≈202 nm, providing

© 2025 The Author(s). Advanced Materials Interfaces published by Wiley-VCH GmbH

21967350, 2025, 22, Downloaded from https://advanced.onlinelibrary.wiley.com/doi/10.1002/admi.202500633 by Ewha Womans University Library, Wiley Online Library on [13/01/2026]. See the Terms and Conditions (https://onlinelibrary.wiley.com/terms-and-conditions) on Wiley Online Library for rules of use; OA articles are governed by the applicable Creative Commons License

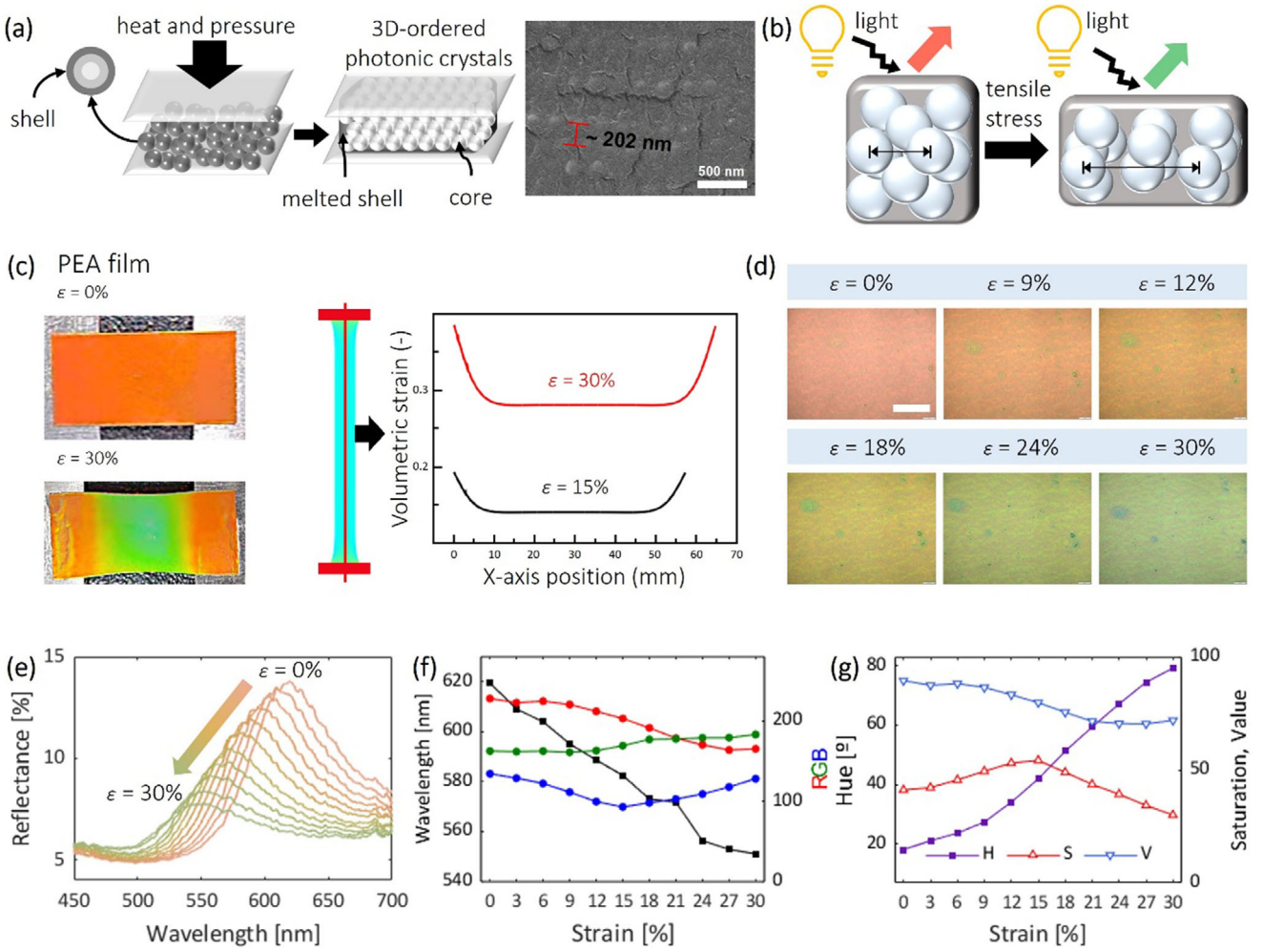


Figure 1. Fabrication and mechanochromic characterization of colloidal photonic crystal (CPC) films. a) Schematic illustration of the melt-shear assembly process used to fabricate the films from core-shell nanoparticles with cross-sectional SEM image ofa PEA-based CPC film. b) Structural color change mechanism: under uniaxial tensile strain (ε), the film stretches along its length while compressing in the thickness direction, reducing interparticle spacing and shifting the reflected wavelength toward shorter wavelengths. c) Photograph of the PEA film under ε = 30% and COMSOL simulation results showing spatial variations in local strain distribution at ε = 15% and ε = 30% global strain. d) Optical images of the PEA film under increasing strain (ε), showing a progressive blue-shift in color. Scale bar, 300 µm. e) Reflectance spectra of the PEA film at different strain levels. f) RGB and peak wavelength (λ) variations with increasing strain. g) HSV color space analysis of the film under strain.

sufficient periodicity for photonic bandgap formation and enabling strain-responsive color shifts. Since the differences in n_{eff} among PEA, PHMA, and PMA are small, the resulting variation in reflected wavelength is minimal under identical strain conditions. Reflectance measurements conducted over the strain range of 0% to 30% yielded similar spectral shifts for all three materials: λ_{PEA} = 619.45 – 551.1 nm, λ_{PHMA} = 598.56 – 535.39 nm, and λ_{PMA} = 593.12 – 499.87 nm (Figure 1e; Figure S3, Supporting Information). The Poisson ratio (ν) of the three CPC films can be approximated from their optical response.[26] Within the strain regime ε ≤ 20%), where the assumptions of constant n_{eff} and isotropic contraction are reasonably valid, we estimate $\nu \approx 0.41$ (PEA), 0.34 (PHMA), and 0.50 (PMA), values consistent with reported ranges for polymer-based photonic crystal films.[27]

Figure 1d demonstrates the strain-dependent color shifts observed in the PEA film. As the tensile stress is applied and the film is progressively stretched, the crystal lattice undergoes compression in the thickness direction. This compression reduces the interparticle spacing within the CPC structure, causing a shift in the wavelength of reflected light, moving toward shorter wavelengths. As a result, the film's color exhibits a blue-shift, transitioning from red or orange colors at low strain levels to green or blue colors at higher strains. Reflectance spectra measurements further confirm this shift, with significant peaks indicating a strong correlation between strain and optical response. As the strain (ε) increases from 0% to 30%, the PEA film's reflected wavelength shifts from approximately 619 nm to 551 nm (Figure 1e). These measurements indicate a clear correlation between the applied strain and the wavelength of reflected light, reinforcing the mechanochromic properties of the PEA film.

While reflectance spectra provides representative wavelength values for the mechanical properties of the films, more detailed

© 2025 The Author(s). Advanced Materials Interfaces published by Wiley-VCH GmbH

21967350, 2025, 22, Downloaded from https://advanced.onlinelibrary.wiley.com/doi/10.1002/admi.202500633 by Ewha Womans University Library, Wiley Online Library on [13/01/2026]. See the Terms and Conditions (https://onlinelibrary.wiley.com/terms-and-conditions) on Wiley Online Library for rules of use; OA articles are governed by the applicable Creative Commons License

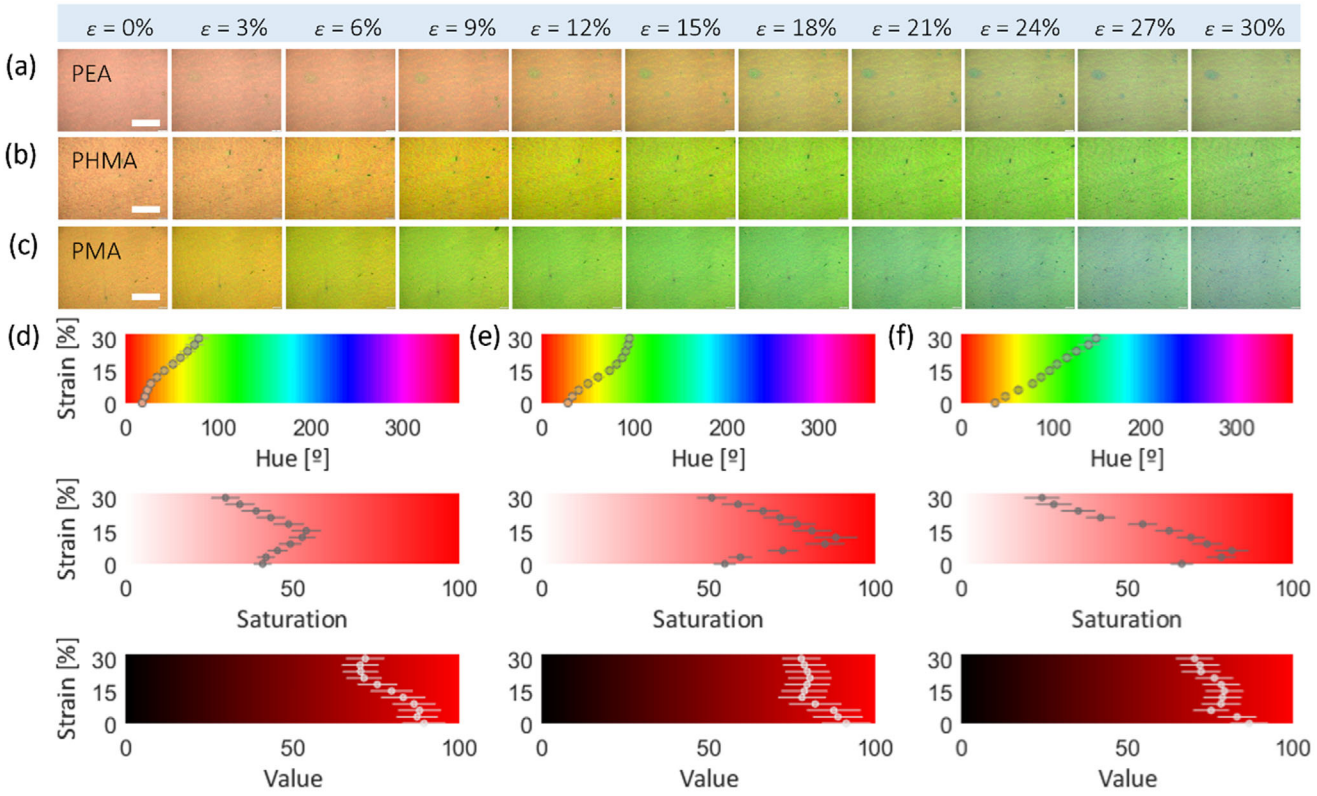


Figure 2. Strain-induced color shifts in three CPC films and their quantification using the HSV color space. Optical images of a) PEA, b) PHMA, and c) PMA films under increasing strain (ε = 0% to 30%), showing a progressive blue-shift due to lattice compression. Scale bar, 300 µm.Quantitative analysis of color changes of d) PEA, e) PHMA, and f) PMA films using the HSV (hue, saturation, value) color space. The top, middle, and bottom rows represent the strain-dependent changes in hue, saturation, and value, respectively.

quantitative color measurements can be obtained from image data. Since image data is typically stored in the RGB format in cameras and displays, the RGB values for each pixel are readily accessible. In our analysis, we extracted the RGB values at each strain step for every pixel in the images, then averaged them over an area of 1200 × 900 µm2 (2592 × 1944 pixels) to ensure reliable measurements; we limited our analysis to the central region of the film (100 cm^2), avoiding edge regions near the clamps where local stress concentration may introduce non-uniform strain (Figure 1c). These average RGB values were plotted as a function of strain, as shown in Figure 1g, giving a comprehensive depiction of the color shifts induced by mechanical deformation. However, as seen in the plots, the RGB values—being composed of three independent components and changing in any of these components—do not correspond linearly to changes in color. This makes it difficult to interpret color shifts using RGB alone, as small changes in strain can lead to complex shifts in multiple RGB components, making direct correlation with strain less intuitive.

To bridge the gap between the quantitative color data and the physical color changes, we transformed the RGB values into HSV color space (S4 in the Supporting Information). In the HSV model, hue directly corresponds to the type of color perceived, while saturation and value represent the color's intensity and brightness, respectively.[28–30] This separation of color characteristics allows for a more focused analysis of the color changes caused by strain. As shown in Figure 1g, the hue component isolates the dominant color change in the strain-induced PEA films and shifts predictably as the lattice periodicity decreases. As strain increases, the blue-shift in the reflected light correlates with a consistent shift in the hue value; specifically, the hue transitions from red to blue as the wavelength of reflected light decreases, aligning closely with human perception of color shifts. This consistency makes hue a more straightforward and quantifiable indicator of strain.[25,31,32]

The strain-responsive color changes in PEA, PHMA, and PMA films at strains ranging from ε = 0% to 30% are shown in **Figure** 2a–c. As strain increases, the films exhibit a progressive blue shift in their reflectance spectra, with PEA shifting from 619 nm to 551 nm, PHMA from 599 nm to 535 nm, and PMA from 593 nm to 500 nm (Figure 1e and Figure S3, Supporting Information); the sensitivities ($\Delta\lambda$/strain) are 2.27 nm/% for PEA, 2.13 nm/% for PHMA, and 3.10 nm/% for PMA. While some composite systems report higher sensitives (≈9.2 nm/% for SiO_2 in poly(ethyl glycol) phenyl ether acrylate), our values are within the typical range for similar CPC platforms (1–4 nm/%, e.g., melt-sheared or PDMS-based).[26,33–36] As CPC optical response is governed by lattice spacing changes, an ideal face-centered-cubic structure with Poisson's ratio 0.5 would exhibit ≈3 nm/% shift under uniaxial strain, and our measured values align well with this expectation while remaining comparable to or exceeding those from similar systems. The gradual fading of the

© 2025 The Author(s). Advanced Materials Interfaces published by Wiley-VCH GmbH

21967350, 2025, 22, Downloaded from https://advanced.onlinelibrary.wiley.com/doi/10.1002/admi.202500633 by Ewha Womans University Library, Wiley Online Library on [13/01/2026]. See the Terms and Conditions (https://onlinelibrary.wiley.com/terms-and-conditions) on Wiley Online Library for rules of use; OA articles are governed by the applicable Creative Commons License

stop-band intensity at higher strains is attributed to lattice densification, which increases particle volume fraction and reduces refractive index contrast between particles and matrix, thereby weakening reflectance.[37]

The corresponding hue (H), saturation (S), and value (V), averaged across all pixels in the images are presented in Figure 2d–f. Although the reflected wavelengths are similar across the films, the absolute hue values differ slightly. This variation can be attributed to subtle differences in the refractive index of the shell polymers, with PEA ($n \approx 1.43$), PHMA ($n \approx 1.431$), and PMA ($n \approx 1.476$), compared with the PS core ($n \approx 1.59$) (Table S3 of the Supporting Information). Using these values within an effective medium approximation for core-shell geometries, n_{eff} of the composites were estimated as 1.522 for PEA, 1.536 for PHMA, and 1.537 for PMA (detailed procedures in S2, Supporting Information). These small but systematic differences in n_{eff} subtly alters how wavelengths are reflected and perceived.[24] These dispersion-related shifts in spectral shape and intensity distribution lead to slight but consistent differences in hue, even at similar peak reflected wavelengths.

To access whether the mechanochromic response depends on film orientation or in-plane anisotropy, we performed axis-dependent testing. Films were cut along three orientations—parallel, perpendicular, and diagonal to the original shearing direction from melt-shere assembly—and subjected to uniaxial strain. As shown in Figure S4 (Supporting Information), all samples exhibited comparable color shifts under identical strain conditions. This result confirms that the optical response is primarily governed by out-of-plane compression affecting the interparticle spacing in the thickness direction. Therefore, even under multi-axial strain, local deformation would be expected to result in similar photonic lattice compression, producing equivalent mechanochromic responses regardless of in-plane direction. Because local deformation under mechanical strain can be calculated via computer simulation, the mechanochromic response is expected to be predictably assessed under multi-axial strain in a facile manner.

We note that, additional light-matter interactions that can influence color perception, such as scattering and absorption, are minimized in our system. Absorption is negligible due to the optical transparency of the acrylate shells, and scattering is mitigated by the monodispersity and local hexagonal ordering of the particles; hexagonal ordering refers to the two-dimensional projection observed from the top surface, corresponding to the (111) plane of a FCC lattice or the (0001) plane of an hexagonal close-packed (hcp) lattice, both of which commonly coexist in colloidal crystals as random hexagonal close-packed (rhcp) structures.[38–41] While some diffuse scattering may still occur, the consistently strong reflectance spectra and vivid structural color (Figure 1e; Figure S3, Supporting Information) indicate that coherent Bragg diffraction is the dominant optical mechanism.[42] Thus, the hue extracted from optical images serves as a reliable and robust indicator of strain-induced structural changes, rather than being significantly affected by extrinsic optical artifacts.

With strain increasing in 3% increments from 0% to 30%, the hue values increase from 18° to 79° for PEA, from 29° to 95° for PHMA, and from 37° to 147° for PMA. The linear relationship between hue and strain highlights the reasonableness of using hue as a reliable indicator of mechanical deformation. Unlike saturation and value, which exhibit overlapping values at different strain levels, hue provides a distinct 1:1 correspondence with strain-induced color shifts. Despite material-dependent offsets in hue, the strain-dependent trends are consistent and reproducible. This direct correlation between hue and the wavelength of reflected light makes it an effective and precise parameter for strain quantification. The corresponding RGB values for PHMA and PMA films at each strain level are provided in Figure S3c and d (Supporting Information), respectively.

Figure S5 (Supporting Information) provides additional data on the linear relationship between strain and hue values in the PEA, PHMA, and PMA films, each exhibiting distinct initial colors at $\varepsilon = 0\%$. As strain increases, the hue values shift linearly, while saturation and value show inconsistent trends across all three films, failing to demonstrate a 1:1 correspondence with strain. This behavior arises from the direct correlation between hue and the wavelength of reflected light, which is governed by the periodicity of the crystal lattice in the films.[43–45] Mechanical strain alters the lattice spacing, inducing a predictable shift in the reflected wavelength that manifests as a color change. The hue component in the HSV color space effectively captures this shift in a linear manner, providing a precise and intuitive correlation between strain and color. This facilitates the translation of observed color changes into measurable strain values. Therefore, hue serves as a reliable and efficient indicator for strain monitoring in mechanochromic materials, offering both accuracy and ease of interpretation. To evaluate the reliability of hue as a strain indicator, we measured hue values of PEA, PHMA, and PMA films at varying strain levels and under two brightness settings: 7 ms and 8 ms for PEA and PMA, and 6 ms and 7 ms for PHMA. **Figure 3**a and b show images of the PEA film at strain levels from $\varepsilon = 0\%$ to 30% under 7 ms and 8 ms exposure times, respectively. Each image comprises 2592 × 1944 pixels, covering an area of 1200 × 900 μm2, from which the hue, saturation, and value components are averaged across all pixels and plotted in Figure 3c–e, respectively. The hue values remained nearly constant across different brightness conditions, demonstrating their robustness as a strain indicator. In contrast, saturation and value exhibited noticeable variations with brightness changes, as they correspond to color intensity and luminance. Despite these variations, the magnitude of change in saturation and value remained consistent across different exposure times, confirming that brightness adjustments primarily affect these two parameters without influencing hue perception. This stability reinforces hue as a reliable strain indicator, independent of lighting conditions. Figures S6 and S7 (Supporting Information) further illustrate similar trends in PHMA and PMA films, where hue values remain consistent under different lighting conditions, supporting the findings in Figure 3.

Since the photonic films do not exhibit uniform hues across all pixels in the images, we analyzed the hue distribution to mitigate any anomalies from the 2592 × 1944 pixels. The hue distributions of the PEA, PHMA, and PMA films are presented in **Figure 4** and Figures S8,S9 (Supporting Information). To refine our measurements, we used a histogram-based outlier detection method, identifying and excluding hues that fell outside the main distribution peak or occurred at low frequencies, which often arise from imaging inconsistencies, minor film defects, or localized artifacts

© 2025 The Author(s). Advanced Materials Interfaces published by Wiley-VCH GmbH

21967350, 2025, 22, Downloaded from https://advanced.onlinelibrary.wiley.com/doi/10.1002/admi.202500633 by Ewha Womans University Library, Wiley Online Library on [13/01/2026]. See the Terms and Conditions (https://onlinelibrary.wiley.com/terms-and-conditions) on Wiley Online Library for rules of use; OA articles are governed by the applicable Creative Commons License

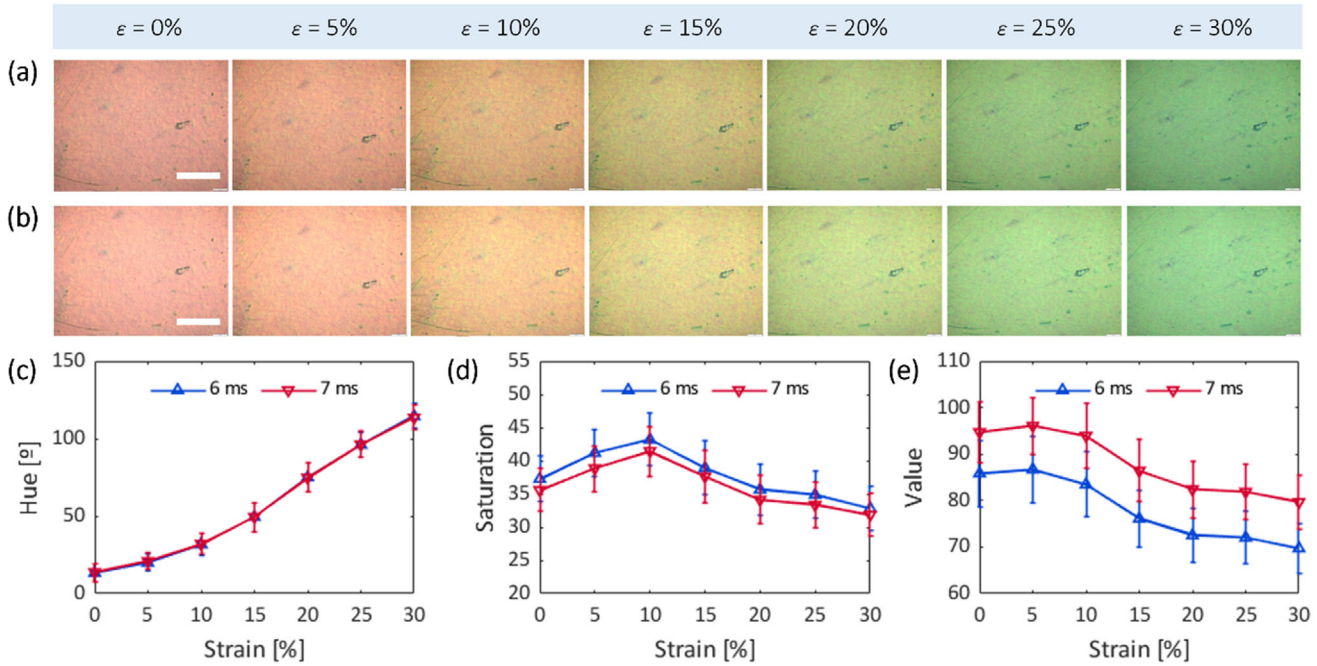


Figure 3. Effect of brightness variation on strain-dependent hue, saturation, and value (HSV) measurements. Optical images of the PEA film at strain levels ranging from ε = 0% to 30% under two different exposure times: a) 7 ms and b) 8 ms. Scale bar, 300 µm. c) Hue, d) saturation, and e) value as a function of strain under different brightness conditions.

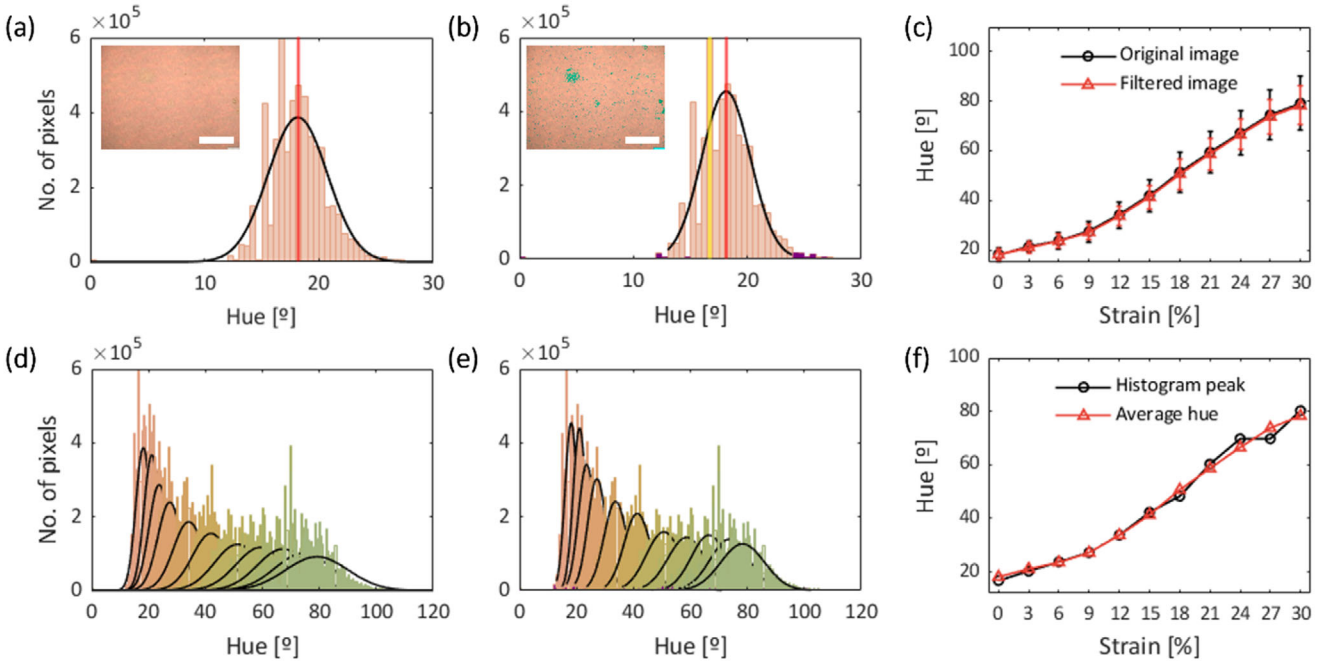


Figure 4. Image filtering on hue distribution of image. Histograms of hue values for the a) original image and b) filtered image at ε = 0%, with corresponding mean hue values of 18.15° and 18.13°, respectively. Insets show the original and filtered images used for analysis. Scale bar, 300 µm. c) Strain-dependent hue measurements for the original and filtered images. d) Histograms of hue values for the original images of PEA and e) filtered hue values. f) Changes in Gaussian peak (average hue) and histogram peak of PEA films under strains ranging from ε = 0% to ε = 30% at $\alpha = 0.03$.

© 2025 The Author(s). Advanced Materials Interfaces published by Wiley-VCH GmbH

21967350, 2025, 22, Downloaded from https://advanced.onlinelibrary.wiley.com/doi/10.1002/admi.202500633 by Ewha Womans University Library, Wiley Online Library on [13/01/2026]. See the Terms and Conditions (https://onlinelibrary.wiley.com/terms-and-conditions) on Wiley Online Library for rules of use; OA articles are governed by the applicable Creative Commons License

21967350, 2025, 22, Downloaded from https://advanced.onlinelibrary.wiley.com/doi/10.1002/admi.202500633 by Ewha Womans University Library, Wiley Online Library on [13/01/2026]. See the Terms and Conditions (https://onlinelibrary.wiley.com/terms-and-conditions) on Wiley Online Library for rules of use; OA articles are governed by the applicable Creative Commons License

like dust and reflections. By carefully setting the threshold, α, we effectively filtered out true anomalies without removing subtle yet relevant hue variations related to strain. This refinement allowed us to focus on consistent hue values across the image, resulting in more accurate strain measurements by minimizing distortions from localized color deviations.

In Figure 4a, the hue distribution of the PEA film at $\varepsilon = 0\%$ is presented, where minor irregularities appear as low-frequency bins outside the main hue distribution peak. The pixel hue values from the image are binned in 1-degree increments, each representing a distinct range. To identify and remove outliers, we applied frequency thresholding, setting the threshold at $\alpha \times$ max(counts), with $\alpha = 0.01$, 0.03, 0.05, 0.07, and 0.1. This process eliminates bins with significantly lower frequencies than the main peaks. In the PEA film, most data points were retained after filtering step. Figure S10 (Supporting Information) shows the PEA films from $\varepsilon = 0\%$ to $\varepsilon = 30\%$ under different α values. At lower α values, outliers are effectively removed, while higher α values risk excluding normal hues, including those critical for representing the effective hue values of the films (Figure S11, Supporting Information). Based on these observations, $\alpha = 0.03$ was determined to provide an optimal balance, effectively filtering outliers while preserving essential hue data (Figure 4e; Figures S8b, and S9b, Supporting Information). The resulting images, with outliers effectively removed, are shown in Figure S10 (Supporting Information), enabling a more consistent analysis by retaining only typical or representative hue values. This improvement in hue consistency is further demonstrated in Figure 4c, where the hue values of the original and filtered images are compared across different strain levels. The two curves show strong agreement, confirming that the filtering process does not distort the overall hue trend while effectively reducing noise. The slightly reduced error bars in the filtered data indicate that extreme outliers have been removed, leading to more stable and reliable hue measurements.

Subtle color variations in the photonic crystal films result in broader hue distributions, as shown in Figure 4; Figures S8,S9, Supporting Information). In Figure 4b, the average actual hue value is 18.15°, which corresponds to the maximum of the Gaussian distribution fit, while the majority of hues are concentrated around 16.75°, as highlighted by the prominent yellow peak.

The hue distribution is unimodal and roughly symmetrical, with a slight mismatch between the average hue and the histogram peak. This discrepancy likely arises from localized color variations caused by minor surface defects or slight inconsistencies in the particle arrangement within the photonic crystal structure.[46,47] Figure 4f summarizes the changes in Gaussian peak (average hue) and histogram peak of PEA films under strains ranging from $\varepsilon = 0\%$ to $\varepsilon = 30\%$ at $\alpha = 0.03$. Since the Gaussian maximum provides a more accurate representation of the dominant hue compared to the pronounced peak in the histogram, it serves as a more reliable metric for quantifying strain-induced color shifts.

To quantitatively describe the chromatic response under mechanical deformation, we analyzed the relationship between average hue (H) and uniaxial strain (ε). As shown in Figure 4 and Figures S8 and S9 (Supporting Information), all three films exhibit a smooth monotonic hue shift with increasing strain. A first-order linear regression yields a physically meaningful and sufficiently accurate description of the hue-strain relationship, with coefficients of determination $R^2 = 0.9778$ for PEA, $R^2 = 0.9597$ for PHMA, and $R^2 = 0.9947$ for PMA, as shown in Figure S12 (Supporting Information). The corresponding linear relations are $H(\varepsilon) = 2.21\varepsilon + 12.11$ for PEA, $H(\varepsilon) = 2.48\varepsilon + 29.55$ for PHMA, and $H(\varepsilon) = 3.60\varepsilon + 40.17$ for PMA. These simple expressions capture the essential dependence of hue on strain and offer a clear physical interpretation. While a higher-order polynomial function (fifth-order) can further improve the statistical fit ($R^2 \geq 0.9995$), its contribution is largely numerical rather than conceptual. Thus, we emphasize the utility of the linear model for describing strain-hue coupling in a concise and physically interpretable manner, with higher-order fitting included only for completeness.

Since hue is directly related to the dominant wavelength of light in the visible spectrum, establishing a strong correlation between hue and wavelength provides a reliable way to monitor and quantify the structural changes in the film. The linear relationship between hue and strain, observed in Figure 2d, demonstrates the effectiveness of hue as a quantitative strain indicator, further validated by its correlation with wavelength. The changes in wavelength and hue for PEA, PHMA, and PMA films at increasing strain are plotted in **Figure 5**a,b, where both exhibit strong linear relationships with strain, confirming their robustness as strain-sensitive metrics. Specifically, the strain-wavelength relations are $\lambda(\varepsilon) = -2.43\varepsilon + 617.25$ for PEA, $\lambda(\varepsilon) = -2.18\varepsilon + 601.92$ for PHMA, and $\lambda(\varepsilon) = -3.07\varepsilon + 593.03$ for PMA. Linear fitting yields coefficients of determination (R^2) close to 1 in all cases, underscoring their reliability of these measurements.

The direct relationship between wavelength (λ) and hue (H) for the three films, as shown in Figure 2 and Figure S5 (Supporting Information), is further analyzed in Figure 5c and Figure S13 (Supporting Information), showing a generally linear trend. However, the degree of correlation varies across the films, reflecting the distinct optical and structural properties of each material. To investigate the material dependence of this relationship, we examined multiple samples and derived film-specific equations. For PEA and PHMA films, well-defined, material-specific relationships between wavelength and hue were observed. Specifically, for two different PEA films, the relationships are given by $\lambda = -1.04H + 628.81$ and $\lambda = -1.13H + 637.23$, while for two different PHMA films, they are $\lambda = -0.85H + 625.96$ and $\lambda = -0.98H + 645.08$. These variations in slope suggest that the rate of wavelength shift per unit hue change is influenced by factors such as refractive index, particle arrangement, and mechanical properties. However, as shown in Figure S13 (Supporting Information), PMA films did not exhibit a consistent hue-wavelength correlation, suggesting that additional factors, such as structural heterogeneity or variations in photonic crystal arrangement, may contribute to deviations from a simple linear trend. The broader distribution of data points of PMA indicates that its mechanochromic response is more complex, potentially due to irregularities in film fabrication or differences in optical resonance mechanisms. Despite these variations, the overall linearity of the hue-wavelength relationships in PEA and PHMA films confirms that image-based hue analysis reliability captures intrinsic optical behavior. This is critical for validating that

 © 2025 The Author(s). Advanced Materials Interfaces published by Wiley-VCH GmbH

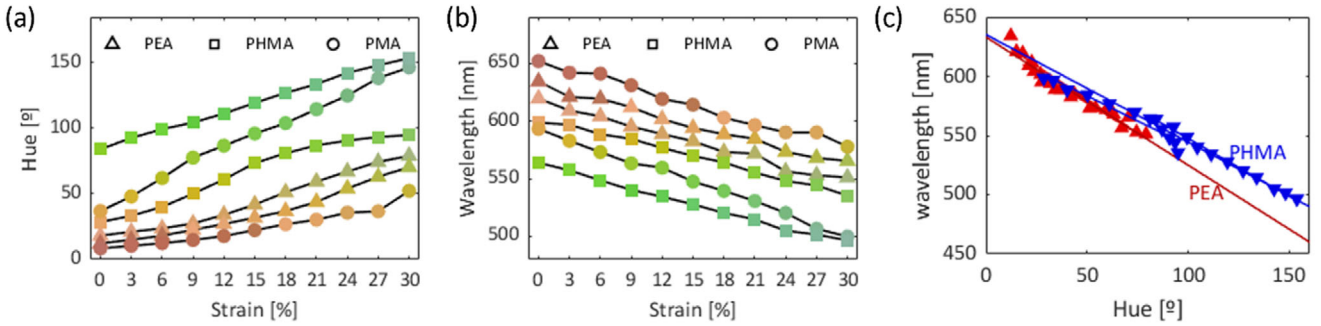


Figure 5. Colorimetric response of PEA, PHMA, and PMA-based photonic materials under mechanical strain. a) The hue angle change with applied strain. b) Corresponding spectral shift in peak wavelength (λ) under strain, demonstrating a systematic decrease in λ with increasing strain. c) Linear correlation between the measured peak wavelength and hue angle for PEA and PHMA films, with the fitted equations confirming a strong relationship between colorimetric parameters.

hue shifts correspond to actual physical deformations in the photonic crystal structure rather than artifacts introduced by image processing. Moreover, the strong linear correlation between hue and strain signifies a constant mechanochromic sensitivity, expressed in terms of both 6.8351nm/% (wavelength shift per unit strain) and 6.0995°/% (hue shift per unit strain). Given this robust correlation, the proposed methodology can be readily extended to other photonic crystal systems or color-shifting materials, broadening its applicability to areas such as strain sensing, tunable optical devices, and material characterization.

Additionally, the reversibility of mechanochromic behavior was evaluated by subjecting the PEA and PHMA films to cyclic stretching and relaxation at $\varepsilon = 15\%$ over five cycles (**Figure 6**a,b). While the PEA, PHMA, and PMA films show breaking strains of ≈677%, ≈350%, and ≈209%, respectively, these crosslinking-free CPC films in this study exhibited plastic deformation beyond a strain threshold determined by the polymer's mechanical properties.[25] For the PMA-based film, plastic deformation began at $\varepsilon = 15\%$, the lowest among the three films. Therefore, we set the reversibility test at $\varepsilon = 15\%$ for the PEA and PHMA samples to ensure consistent and comparable conditions. Wavelength changes were compared between direct measurements from reflectance spectra and wavelength values extracted from hue analysis (Figure 6c). Directly measured reflectance data showed variations of 628.7 ± 3.15 nm at $\varepsilon = 0\%$ and 589.66 ± 2.27 nm at $\varepsilon = 15\%$. In contrast, wavelength changes estimated from hue changes in the image analysis provided more consistent values, with variations of 624.32 ± 0.68 nm at $\varepsilon = 0\%$ and 589.71 ± 1.42 nm at $\varepsilon = 15\%$. These hue-derived results closely match the directly measured values, with differences within experimental uncertainty, confirming that hue analysis accurately captures strain-induced color shifts and provides a reliable approximation of optical changes.

The smaller deviations observed in hue-derived wavelength measurements further highlight the measurement precision, which translates into improved strain resolution. Using the measured hue accuracies ($\sigma = 0.718°$ for PEA and $\sigma = 0.332°$ for PHMA) and hue-strain slopes (-2.03°/% and -2.21°/%), the strain resolution, calculated as $\sigma/|\Delta\text{hue}/\text{strain}|$, is ≈0.35% for PEA and ≈0.15% for PHMA. This demonstrates that hue-resolved quantification can detect smaller strain changes than would be practical with direct spectral tracking. The resolution can be further improved through temporal and spatial averaging, where the uncertainty decreases according to $\sigma_{avg} = \sigma/\sqrt{N}$. While reflectance spectra directly capture optical shifts, they are more susceptible to experimental noise and variations in the optical setup, which can affect reproducibility. In comparison, hue-based analysis mitigates such inconsistencies by averaging pixel data over the entire film area, providing a more stable estimate of wavelength changes. This consistency demonstrates the robustness of hue analysis for monitoring reversible mechanochromic behaviors, making precise and scalable method for applications requiring reliable strain sensing.

In the broader context of mechanochromic photonic materials, the three CPC films studied here (PEA, PHMA, and PMA) exhibit optical responses in the visible range ($\lambda \approx$ 500–650 nm), generally comparable to reported values for distributed Bragg reflectors, liquid-crystal-based structures, and inverse opals.[26,48,49] The estimated optical Poisson ratios ($\nu \approx$ 0.34–0.50) also align with typical ranges for polymer-based photonic crystals,[26] supporting the validity of our structural interpretation. At the same time, material-specific differences are evident, reflecting variations in shell composition and modulus. While mechanochromic sensitivity and working spectral range have been investigated across different photonic architectures, the hue-resolved image analysis applied here provides a distinctive advantage by directly correlating lattice compression with optical shifts. This situates CPC films as not only representative model systems but also versatile platforms for extending mechanochromic sensing strategies to diverse photonic crystal structures.

3. Conclusion

This study introduces an image-based quantification method for analyzing the mechanochromic behaviors in soft CPC films. By converting RGB image data into the HSV color space, we successfully isolated hue as a precise and reliable indicator of strain, directly correlating with the wavelength shifts caused by lattice periodicity changes under mechanical deformation. A consistent linear relationship between hue and strain across different material compositions (PEA, PHMA, and PMA films) underscores the

© 2025 The Author(s). Advanced Materials Interfaces published by Wiley-VCH GmbH

21967350, 2025, 22, Downloaded from https://advanced.onlinelibrary.wiley.com/doi/10.1002/admi.202500633 by Ewha Womans University Library, Wiley Online Library on [13/01/2026]. See the Terms and Conditions (https://onlinelibrary.wiley.com/terms-and-conditions) on Wiley Online Library for rules of use; OA articles are governed by the applicable Creative Commons License

robustness of this approach. Unlike conventional spectroscopy, this method provides a scalable, cost-effective alternative for evaluating structural color in mechanochromic systems. Histogram-based thresholding enhances measurement accuracy by filtering noise, while the stability of hue under varying brightness conditions ensures reliability in real-world environments. Importantly, our results demonstrate that hue-strain correlations reliably capture lattice compressions at the material-interface level, establishing hue as a robust and physically meaningful optical readout of CPC film deformation. This framework opens new avenues for wearable strain sensors, industrial monitoring systems, and material characterization. By enabling hue extraction from individual video frames, the method allows continuous, in-situ strain quantification, enhancing its suitability for real-time monitoring. Future optimization could further improve environmental adaptability through long-cycle fatique and environmental stability tests, supporting broader integration of mechanochromic materials in smart sensing technologies.

Supporting Information

Supporting Information is available from the Wiley Online Library or from the author.

Acknowledgements

This research was financially supported by the Institute of Civil Military Technology Cooperation (No.22-CM-C0-01) funded by the Defense Acquisition Program Administration and Ministry of Trade, Industry and Energy and National Research Foundation of Korea (NRF) Grant funded by the Korean government (MSIT) (No. RS-2025-02215502).

Conflict of Interest

The authors declare no conflict of interest.

Author Contributions

Y.L. conducted the primary data analysis and S.L. contributed image-based analysis. C.Y.O. performed the experiments under the guidance of T.S.S. H.H. led and supervised the entire research project. All authors contributed to writing and reviewing the manuscript.

Data Availability Statement

The data that support the findings of this study are available from the corresponding author upon reasonable request.

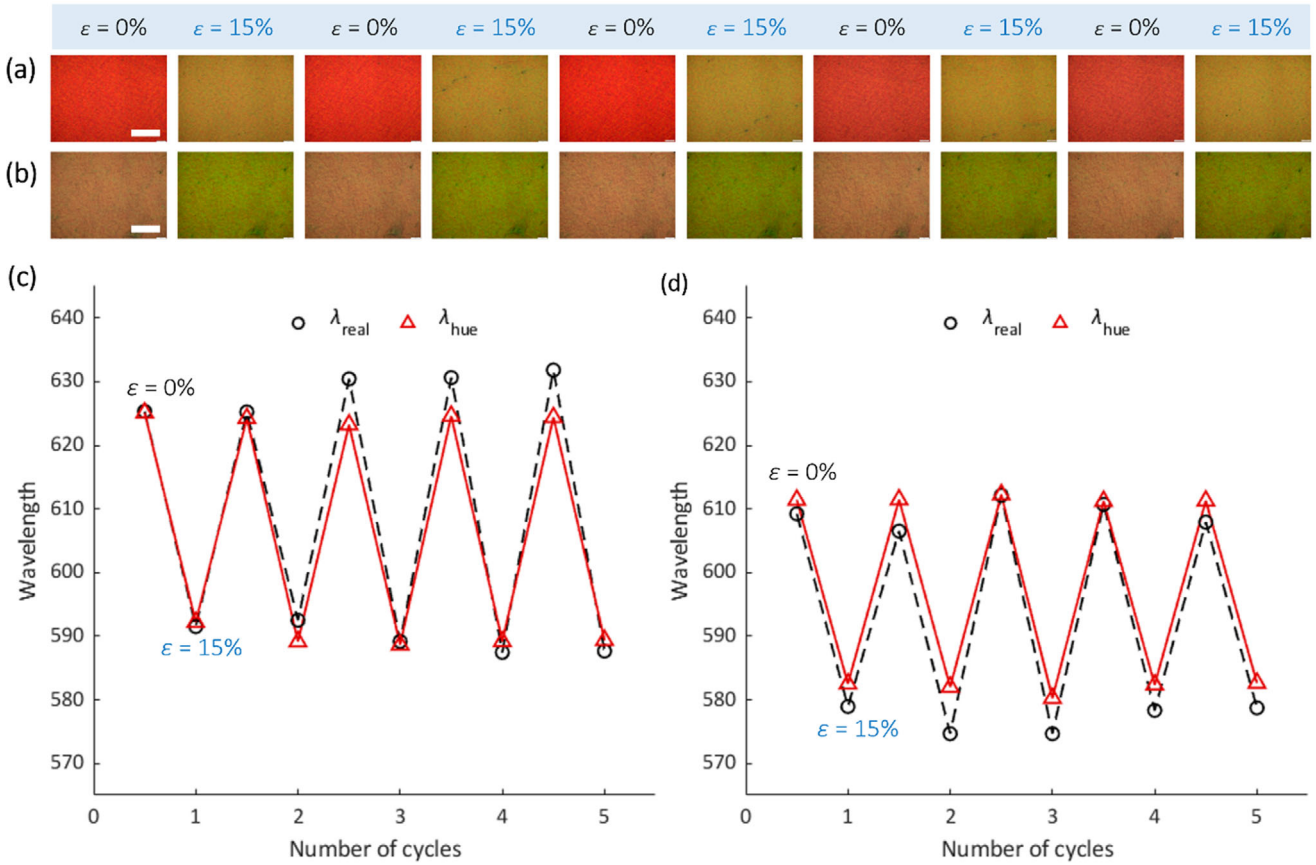


Figure 6. Reversible colorimetric response of photonic films under cyclic mechanical strain. Sequential images of the a) PEA and b) PHMA films at ε = 0% and 15% strain, showing a reversible color change between red and green. Scale bar, 300 μm. c) Plots of the measured peak wavelength (λ_{real}) and the estimated wavelength from hue (λ_{hue}) over five stretching cycles for (c) PEA and d) PHMA films, demonstrating consistent and repeatable shifts in optical properties.

© 2025 The Author(s). Advanced Materials Interfaces published by Wiley-VCH GmbH

21967350, 2025, 22, Downloaded from https://advanced.onlinelibrary.wiley.com/doi/10.1002/admi.202500633 by Ewha Womans University Library, Wiley Online Library on [13/01/2026]. See the Terms and Conditions (https://onlinelibrary.wiley.com/terms-and-conditions) on Wiley Online Library for rules of use; OA articles are governed by the applicable Creative Commons License

Keywords

colloidal photonic crystals, digital image analysis, hue-wavelength relationship, mechanochromic materials, strain sensing

Received: July 11, 2025
Revised: September 5, 2025
Published online: September 16, 2025

[1] H.-Y. Lee, M. Gu, J. Hwang, H. Hwang, Y.-S. Kim, S. Y. Lee, S.-H. Kim, *Adv. Sci.* **2024**, *11*, 2304022.
[2] P. Snapp, P. Kang, J. Leem, S. Nam, *Adv. Funct. Mater.* **2019**, *29*, 1902216.
[3] P. Wu, X. Shen, C. G. Schäfer, J. Pan, J. Guo, C. Wang, *Nanoscale* **2019**, *11*, 20015.
[4] R. Zhang, Q. Wang, X. Zheng, *J. Mater. Chem. C* **2018**, *6*, 3182.
[5] S. Kinoshita, S. Yoshioka, *ChemPhysChem* **2005**, *6*, 1442.
[6] E. Yablonovitch, *Sci. Am.* **2001**, *285*, 46.
[7] P. Vukusic, J. R. Sambles, *Nature* **2003**, *424*, 852.
[8] R. Zhao, Y. He, Y. He, Z. Li, M. Chen, N. Zhou, G. Tao, C. Hou, *ACS Appl. Mater. Interfaces* **2023**, *15*, 16063.
[9] J. Chen, L. Xu, M. Yang, X. Chen, X. Chen, W. Hong, *Chem. Mater.* **2019**, *31*, 8918.
[10] M. H. Barbee, K. Mondal, J. Z. Deng, V. Bharambe, T. V. Neumann, J. J. Adams, N. Boechler, M. D. Dickey, S. L. Craig, *ACS Appl. Mater. Interfaces* **2018**, *10*, 29918.
[11] J. H. Shin, J. Y Park, S. H. Han, Y. H. Lee, J.-Y. Sun, S. S Choi, *Adv. Sci.* **2022**, *9*, 2202897.
[12] S. H. Han, J. H. Shin, H. J. Yang, S. Nam, J. Y Park, S. S Choi, *Adv. Sci.* **2025**, *12*, 2408346.
[13] C. Kwon, S. Nam, S. H. Han, S. S Choi, *Adv. Funct. Mater.* **2023**, *33*, 2304506.
[14] L. Zheng, N. Li, C. Qi, D. Ma, D. Yang, S. Huang, *ACS Appl. Mater. Interfaces* **2025**, *17*, 11020.
[15] R. Yang, W. Cheng, X. Chen, Q. Qian, Q. Zhang, Y. Pan, P. Duan, P. Miao, *ACS Omega* **2018**, *3*, 12141.
[16] Y. Jung, J. Kim, O. Awofeso, H. Kim, F. Regnier, E. Bae, *Appl. Opt.* **2015**, *54*, 9183.
[17] V. Kılıç, G. Alankus, N. Horzum, A. Y. Mutlu, A. Bayram, M. E. Solmaz, *ACS Omega* **2018**, *3*, 5531.
[18] L. D. Bonifacio, D. P. Puzzo, S. Breslav, B. M. Willey, A. McGeer, G. A. Ozin, *Adv. Mater.* **2010**, *22*, 1351.
[19] W. Zhang, L. Qiu, K. J. Shea, J. Fan, Y. Liu, W. Zheng, M. Xue, W. Liu, Z. Xu, X. E., X. Dong, Y. Qiao, Z. Meng, *ACS Appl. Mater. Interfaces* **2022**, *14*, 35010.
[20] H. Chen, J. Wei, F. Pan, T. Yuan, Y. Fang, Q. Wang, *Adv. Mater. Technol.* **2025**, *10*, 2400865.
[21] S.-Y. Leo, W. Zhang, Y. Zhang, Y. Ni, H. Jiang, C. Jones, P. Jiang, V. Basile, C. Taylor, *Small* **2018**, *14*, 1703515.
[22] Yi Yang, L. Yu, X. Jiang, Y. Li, X. He, L. Chen, Y. Zhang, *Chem. Commun.* **2024**, *60*, 9177.
[23] J. E. Fröch, L. Huang, Z. Zhou, V. Tara, Z. Fang, S. Colburn, A. Zhan, M. Choi, A. Manna, A. Tang, Z. Han, K. F. Böhringer, A. Majumdar, *Light: Sci. Appl.* **2025**, *14*, 217.
[24] C. Y. Oh, J. S. Kim, T. S. Shim, *Adv. Opt. Mater.* **2024**, *12*, 2401382.
[25] Y. Cho, C. Y. Oh, E. J. Son, Y.-S. Kim, T. S. Shim, *Adv. Opt. Mater.* **2024**, *12*, 2400135.
[26] M. Martusciello, A. Lanfranchi, M. Castellano, M. Patrini, P. Lova, D. Comoretto, *ACS Appl. Mater. Interfaces* **2024**, *16*, 51384.
[27] H. Li, X. Sun, H. Peng, *ChemPhysChem* **2015**, *16*, 3761.
[28] G. H. Joblove, D. Greenberg, *Comput. Graph.* **1978**, *12*, 20.
[29] K. Cantrell, M. M. Erenas, I. de Orbe-Payá, L. F. Capitán-Vallvey, *Anal. Chem.* **2010**, *82*, 531.
[30] N. A. Ibraheem, M. M. Hasan, R. Z. Khan, P. K. Mishra, *ARPN J. Sci. Technol.* **2012**, *2*, 265.
[31] M. Anderson, R. Motta, S. Chandrasekar, M. Stokes, *Color Imag. Conf.* **1996**, *4*, 238.
[32] Y. Zhao, K. Zhao, Z. Yu, C. Ye, *Polymers* **2023**, *15*, 2635.
[33] T. Winter, A. Boehm, V. Presser, M. Gallei, *Macromol. Rapid Commun.* **2021**, *42*, 2000557.
[34] S. H. Foulger, P. Jiang, A. C. Lattam, D. W. Smith, J. Ballato, *Langmuir* **2001**, *17*, 6023.
[35] D. Scheid, C. Lederle, S. Vowinkel, C. G. Schäfer, B. Stühn, M. Gallei, *J. Mater. Chem. C* **2014**, *2*, 2583.
[36] N. Sitpathom, T. Muangnapoh, J. M. Dawes, *Opt. Express* **2020**, *28*, 16280.
[37] G. H. Lee, T. M. Choi, B. Kim, S. H. Han, J. M. Lee, S.-H. Kim, *ACS Nano* **2017**, *11*, 11350.
[38] A. V. Petukhov, I. P. Dolbnya, D. G. A. L. Aarts, G. J. Vroege, H. N. W. Lekkerkerker, *Phys. Rev. Lett.* **2003**, *90*, 028304.
[39] A. G. Shabalin, J.-M. Meijer, R. Dronyak, O. M. Yefanov, A. Singer, R. P. Kurta, U. Lorenz, O. Y. Gorobtsov, D. Dzhigaev, S. Kalbfleisch, J. Gulden, A. V. Zozulya, M. Sprung, A. V. Petukhov, I. A. Vartanyants, *Phys. Rev. Lett.* **2016**, *117*, 138002.
[40] I. P Dolbnya, A. V Petukhov, D. G. A. L Aarts, G. J Vroege, H. N. W Lekkerkerker, *Europhys. Lett.* **2005**, *72*, 962.
[41] I. Sanchez-Burgos, E. Sanz, C. Vega, J. R. Espinosa, *Phys. Chem. Chem. Phys.* **2021**, *23*, 19611.
[42] Y. Xia, B. Gates, Y. Yin, Y. Lu, *Adv. Mater.* **2000**, *12*, 693.
[43] G. Wyszecki, W. S. Stiles, in *Color Science: Concepts and Methods, Quantitative Data and Formulae*, (2nd Ed.), John Wiley & Sons, New York **1982**, p. 950.
[44] A. Battisti, P. Minei, A. Pucci, R. Bizzarri, *Chem. Commun.* **2017**, *53*, 248.
[45] X. Sun, J. Zhang, X. Lu, X. Fang, H. Peng, *Angew. Chem., Int. Ed.* **2015**, *54*, 3630.
[46] C. Li, M. Zhao, X. Zhou, H. Li, Y. Wang, X. Hu, M. Li, L. Shi, Y. Song, *Adv. Opt. Mater.* **2018**, *6*, 1800651.
[47] H. S. Lee, T. S. Shim, H. Hwang, S.-M. Yang, S.-H. Kim, *Chem. Mater.* **2013**, *25*, 2684.
[48] H. Finkelmann, S. T. Kim, A. Muñoz, P. Palffy-Muhoray, B. Taheri, *Adv. Mater.* **2001**, *13*, 1069.
[49] H. Megahd, P. Lova, D. Comoretto, *Adv. Funct. Mater.* **2021**, *31*, 2009626.

© 2025 The Author(s). Advanced Materials Interfaces published by Wiley-VCH GmbH

21967350, 2025, 22, Downloaded from https://advanced.onlinelibrary.wiley.com/doi/10.1002/admi.202500633 by Ewha Womans University Library, Wiley Online Library on [13/01/2026]. See the Terms and Conditions (https://onlinelibrary.wiley.com/terms-and-conditions) on Wiley Online Library for rules of use; OA articles are governed by the applicable Creative Commons License